Computational and Structural Biotechnology Journal 21 (2023) 688–701

Contents lists available at ScienceDirect

Computational and Structural Biotechnology Journal

journal homepage: www.elsevier.com/locate/csbj

Structure-based discovery and in vitro validation of inhibitors of chloride intracellular channel 4 protein

Fisayo Olotu [a], Encarnacion Medina-Carmona [b,c], Angela Serrano-Sanchez [b], Felipe Ossa [d], Abdelaziz El-Hamdaoui [d], Özlem Tastan Bishop [a], Jose L. Ortega-Roldan [b], Vahitha B. Abdul-Salam [d,*]

[a] Research Unit in Bioinformatics (RUBi), Department of Biochemistry and Microbiology, Rhodes University, Makhanda 6139, South Africa
[b] School of Biosciences, University of Kent, CT2 7NJ Canterbury, United Kingdom
[c] Departamento de Quimica-Fisica, Facultad de Ciencias, Universidad de Granada, Spain
[d] Centre for Cardiovascular Medicine and Device Innovation, William Harvey Research Institute, Barts and The London School of Medicine and Dentistry, Queen Mary University of London, United Kingdom

ARTICLE INFO

Article history:
Received 10 June 2022
Received in revised form 22 December 2022
Accepted 23 December 2022
Available online 24 December 2022

Keywords:
Chloride intracellular channel protein 4
GSH-like catalytic site
Structure-based drug discovery
Computational high-throughput screening
Nuclear magnetic resonance
Allosteric inhibition

ABSTRACT

The use of computer-aided methods have continued to propel accelerated drug discovery across various disease models, interestingly allowing the specific inhibition of pathogenic targets. Chloride Intracellular Channel Protein 4 (CLIC4) is a novel class of intracellular ion channel highly implicated in tumor and vascular biology. It regulates cell proliferation, apoptosis and angiogenesis; and is involved in multiple pathologic signaling pathways. Absence of specific inhibitors however impedes its advancement to translational research. Here, we integrate structural bioinformatics and experimental research approaches for the discovery and validation of small-molecule inhibitors of CLIC4. High-affinity allosteric binders were identified from a library of 1615 Food and Drug Administration (FDA)-approved drugs via a high-performance computing-powered blind-docking approach, resulting in the selection of amphotericin B and rapamycin. NMR assays confirmed the binding and conformational disruptive effects of both drugs while they also reversed stress-induced membrane translocation of CLIC4 and inhibited endothelial cell migration. Structural and dynamics simulation studies further revealed that the inhibitory mechanisms of these compounds were hinged on the allosteric modulation of the catalytic glutathione (GSH)-like site loop and the extended catalytic β loop which may elicit interference with the catalytic activities of CLIC4. Structure-based insights from this study provide the basis for the selective targeting of CLIC4 to treat the associated pathologies.

Abbreviations: A9C, 9-Anthracenecarboxylic acid; Ad, Adenovirus; AMPhB, Amphotericin B; Bad, BCL2 associated agonist of cell death; Bcl-2, B-cell lymphoma 2; Bcl-xL, B-cell lymphoma-extra large; CDK, Cyclin-dependent kinases; CLIC, Chloride intracellular channel protein; DAPI, 4′,6-diamidino-2-phenylindole; DIDS, 4,4′-Diisothiocyano-2,2′-stilbenedisulfonic acid; DMSO, Dimethyl sulfoxide; DOPE, Discrete optimized protein energy; GPU, Graphics Processing Unit; GST, glutathione S-transferases; GUI, Graphical User Interface; HEPES, (4-(2-hydroxyethyl)− 1-piperazineethanesulfonic acid;; HIF, Hypoxia-inducible factor; HSQC, Heteronuclear single quantum coherence spectroscopy; HUVEC, Human umbilical vein endothelial cells; IKKβ, Inhibitor of nuclear kappa-B-kinase subunit beta; JNK, c-Jun N-terminal kinase; MKK6, Mitogen-activated protein kinase kinase-6; MOI, Multiplicity of infection; NaCL, Sodium chloride; NF-κB, Nuclear factor kappa-light-chain-enhancer of activated B cells; NMR, Nuclear magnetic resonance; NPT, The constant-temperature, constant-pressure ensemble; p38, Mitogen activated protein kinases; PAH, Pulmonary arterial hypertension; RAPA, Rapamycin; SASA, Solvent accessible surface area; SEK1, Dual specificity mitogen-activated protein kinase kinase 4; Smad, Suppressor of Mothers against Decapentaplegic; TEV, Tobacco etch virus; TIP3P, Transferable intermolecular potential 3 P; TROSY, Transverse relaxation optimized spectroscopy; UCSF, University of California, San Francisco; VEGF, Vascular endothelial growth factor

* Correspondence to: Centre for Cardiovascular Medicine and Device Innovation, William Harvey Research Institute, Faculty of Medicine and Dentistry, Queen Mary University of London, Charterhouse Square, London EC1M 6BQ, United Kingdom.
E-mail address: v.abdulsalam@qmul.ac.uk (V.B. Abdul-Salam).

https://doi.org/10.1016/j.csbj.2022.12.040

1. Introduction

Despite ion channel drugs being almost 18% of currently marketed medications with an estimated global sale of £ 10 billion, the development of newer drugs, especially for chloride channels, is still lagging. This is mainly due to the lack of efficient pharmacological pipelines targeting these proteins and an incomplete understanding of their precise mechanisms in biological systems [1]. Chloride intracellular channel 4 (CLIC4) belongs to the highly conserved six-membered family of globular proteins (CLIC1–6) which structurally relate to the omega-class glutathione S-transferases (GSTΩs) [2]. Functionally, CLIC proteins are not conventional chloride channels and as well do not function similarly to GST proteins, hence, the majority of their activities do not depend on their roles as channel proteins [2,3]. CLICs are globular proteins and have been associated to varieties of multiorganelle/cellular processes, some of which include tubulogenesis, membrane remodeling, endosomal trafficking, vacuole formation, and cell adhesion [3–6]. Particularly, CLIC4 is homogenously distributed in the cytosol and exhibits glutaredoxin-like glutathione-dependent oxidoreductase enzyme activity [7]. In the presence of activating molecules (agonists), CLIC4 translocates rapidly and reversibly from the cytosol to the plasma membrane, with the involvement of G-actin-binding protein profilin 1 and actin polymerization induced by Rho and mammalian Diaphanous (mDia) 2 (mDia2) formin [8,9]. Several studies have reported the dynamic association of CLIC4 with effector proteins in the cytosol as well as in the plasma membrane. CLIC4 has been shown to localize in lipid rafts where it interacts with ezrin-radixin-moesin (ERM) proteins that connects receptor proteins in the membrane with submembrane actin cytoskeleton [10]. Its association with β_1 integrin also accounts for its modulatory roles in cell adhesion, and migration [11]. Furthermore, CLIC4 reportedly functions as a scaffold for protein kinases and phosphatases and therefore plays crucial role in the phosphorylation of signaling proteins such CDK2 and CDK6, Smad2/3, p38, IKKβ, MKK6, JNK and SEK1 [3,12]. CLIC4 localization and modulatory activities have been reported in the lungs [13] and bone marrow [14] as well as in several cellular types and intracellular organelles [2] which could explain its significance in multiple cellular and physiological processes.

As a result of its metamorphic roles, CLIC4 has been implicated in various pathophysiological pathways [15]. For instance, it is well-characterized for its roles in cancer [12,15,16] and pulmonary arterial hypertension (PAH) [13,17]. Studies have revealed that CLIC4 regulates multiple stages of angiogenesis and acts upstream of hypoxia-inducible factor (HIF-1α) and vascular endothelial growth factor (VEGF) signaling that drives the onset of oxidative stress. This could explain its increased expression in many cancers presenting it as a target for the development of novel cancer therapeutics [16,18,19]. Suppressing CLIC4 has been shown to decrease cell proliferation, capillary network formation, capillary-like sprouting, and lumen formation in tumor cells [20,21]. Also, inhibiting CLIC4 correlatively enhanced the phosphorylation of Bcl-2, Bcl-xL and Bad which in turn increased β-cell survival and cytokine-mediated apoptotic resistance [22]. Similarly, reducing *clic4* expression and blocking downstream interactions may provide a novel way to prevent diabetes-related β-cell apoptosis. More so, CLIC4 was highly expressed in the lungs of patients with pulmonary arterial hypertension (PAH) as compared to healthy patients [13] and regulated the activities of the transcription factors, NF-κB and HIF-1, that are responsible for endothelial responses to inflammatory and angiogenic stimuli.

Several attempts have been made to achieve and translate the pharmacological inhibition of CLIC4 for disease treatment but have been unsuccessful to date. This, among many others may be due to its high structural and sequence similarity with other non-pathogenic CLIC proteins as well as the GSTΩs [7,22]. Small-molecule inhibition of overexpressed CLIC proteins has been commonly achieved with the use of indanyloxyacetic acid-94 (IAA94), an intracellular chloride channel blocker designed based on the GST inhibitor, ethacrynic acid [23]. This compound however lacks specificity and binds with various members of the CLIC family (SspA, CLIC1, CLIC3, CLIC4, and CLIC5) [16,24,25] and other chloride channels family of proteins such as pannexin1 [26], bestrophin [27], Calcium-activated chloride channels, Volume regulated anion channels (VRAC) [28] not particularly involved in disease development. Other known chloride channel blockers such as A9C and DIDS have been tested on CLICs where only A9C but not DIDS is known to act on CLICs [29]. A9C was recently shown to also inhibit the enzymatic activity of CLICs [7]. Pharmacological inhibition of CLICs by IAA94 is shown to reduce tumor growth as well as prevent neurodegeneration [30]. Moreover, given the functional versatility of the various CLICs and the non-specific activities of IAA94 and A9C, future research is needed to focus on chemical derivatives or new molecules with improved specificity.

The crystal structure availability of the soluble form of CLIC4 provides an advantage that can be exploited using *in silico* structure-based techniques. Therefore, in this study we implemented integrative computer-based and experimental methods to: (i) identify new druggable allosteric sites on CLIC4; (ii) blind-screen and discover hit inhibitor compounds specific for CLIC4; (iii) validate the inhibitory potentials of the hit compounds in vitro (iv) investigate CLIC4 allosteric inhibitory mechanisms using GPU-accelerated molecular dynamics (MD) simulations. We expect that findings from this study will contribute significantly to therapeutic interventions in various CLIC4-mediated pathologies.

2. Computational methodology

2.1. Retrieval of the protein three-dimensional structure and preparation

The three-dimensional (3D) structure of CLIC4 was obtained from the Protein Data Bank (PDB) with entry 2AHE [31], and was prepared for subsequent analyses on the graphic user interface (GUI) of UCSF Chimera [32]. This structure contains missing residues particularly at the flexible foot loop (FFL) region (residues 158–175) which we hypothesize could be important allosteric site for CLIC4 targeting among other possible sites. Other available CLIC4 PDB structure (2D2Z) were also devoid of this region due to crystal disorder. Therefore to model only this missing region, we employed a homologous CLIC1 structure that has a crystal resolved FFL (~70% identity; PDB 1K0M [33]) as a partial template in an ad hoc structural modeling pipeline implemented using MODELLER v10.1. The normalized DOPE (z-DOPE) scores were then used to select the best CLIC4 structural model (consisting the FFL). For comparative modeling and analysis, the 3D structure of the CLIC1 homolog complexed with glutathione (GSH) was also obtained from PDB with entry 1K0N [34]. This was done so as to correctly map out the GSH-binding region which is reportedly highly conserved in all human CLIC homologs, particularly the catalytic cysteine [5]. System preparation involved the removal of co-crystallized molecules such as crystal waters from both proteins, and the non-GSH binding monomer from CLIC1. More so, both CLICs were structurally superposed using Needleman-Wunsch algorithm (UCSF Chimera MatchMaker) to define the GSH binding region in CLIC4. This implemented a pairwise alignment of the sequences which were then fitted per aligned-residue pair. CLIC4 residues at a distance of 5 Å from the crystal GSH

were mapped accordingly to constitute the GSH-binding region in CLIC4.

2.2. Identification, cross-validation and characterization of potential allosteric sites

Multiple predictive algorithms were implemented to identify possible allosteric sites on CLIC4 asides the GSH-binding region mapped in section ***1.1***. This approach is in line with some previous studies [33,35–38] and important to predict consensus sites (across the algorithms) with high potentials for druggability. Tools employed for allosteric site prediction and characterization in this study include SiteMap [39], DeepSite [40], FTMap [41], DogSiteScore [42], and ProBIS [43]. The targetability of allosteric pockets predicted by SiteMap is further based on properties that include surface exposure, hydrophobicity, hydrophilicity, and druggability, as measured by the Halgren's and DogSite scores [39]. The consensus allosteric pocket as commonly predicted across the five algorithms was then mapped and characterized based on these intrinsic attributes.

2.3. Computational high-throughput screening and hit identification

A library of 1615 FDA approved compounds was retrieved from the ZINC15 repository (http://zinc15.docking.org/substances/subsets/fda/), with each constituent compounds subjected to structural optimization, protonation and energy minimization using Open Babel and AutoDock tools for the final conversion into *.pdbqt* formats. The prepared ligands were allowed to be flexible and then used to the screen the target protein (rigid) across its entire surface. This is a blind docking approach which allows small-molecule compounds to 'non-restrictively' bind to preferred sites on their target proteins based on affinity and interaction complementarity. In addition, this approach is important to further validate the potential druggability of pockets predicted in section ***1.2***. UCSF Chimera-integrated AutoDock Vina was used to calculate the docking coordinates which include box sizes *x*, *y*, *z*; 47.73, 53.92, 60.38 and centers *x*, *y*, *z*; − 2.46, − 12.84, 29.82. As a positive control, IAA94, a widely reported 'non-selective' CLIC inhibitor was blindly docked to CLIC4 using the same coordinates, since the exact IAA94 binding site on CLIC4 has not been clearly defined. The screening experiment was then performed using AutoDock Vina integrated in a high-performance computing (HPC) cluster. The resulting docked poses of the inhibitor compounds with respect to their scores were visualized in PyMOL GUI after which they were filtered based on their binding energies (affinity), non-preferentially to the GSH binding site and ultimately, their pharmacological relevance (usage). Taken together, the top 10 hits with potential allosteric selectivity for CLIC4 were selected for further evaluation.

2.4. Molecular dynamics (MD) simulations of protein systems

Following in vitro validative experiments for the predicted hits, two inhibitor-protein complexes together with the unbound and IAA94-bound proteins (controls) were prepared for long-timescale MD simulations. This was carried out on the AMBER18 Graphical Processing Unit (GPU) and its integrated modules [44]. The FF14SB forcefield was used to define the protein parameters and antechamber/parmchk modules for ligand parameterization. Likewise, coordinate and topology files for the unbound and inhibitor-bound proteins were defined with the LEaP program. This program, also, was used to add counter Na^+ and Cl^- ions to neutralize and solvate the systems in a TIP3P water box extending10Å from the solute. Partial minimization was first carried out for 5000steps using a 500 kcal/mol.$Å^2$ restraint potential followed by another 2500 steps of full minimization without restraints. The systems were then heated in a canonical (NVT) ensemble with a 5 kcal/mol $Å^2$ harmonic restraints gradually from 0 to 300 K for 50 ps, followed by a 250,000 equilibration steps in an NPT ensemble at constant temperature of 300 K without restraints. Atmospheric pressure was maintained at 1 bar with a Berendsen barostat [45] while each protein system was subjected to a production run of 500 ns. Corresponding trajectories were saved at every 1 ps time-frame until the end of the simulation and were analysed using CPPTRAJ followed by data plot analyses using Microcal Origin software [46] and an in-house R-script. Snapshots were also taken and analyzed to monitor structural events and ligand interaction dynamics across the trajectories on UCSF Chimera user interface (GUI), PyMOL and Discovery Studio Client. [47].

2.5. Calculations of binding free energies and per-residue decomposition

Differential binding affinities of the validated allosteric CLIC4 inhibitors and control compound were evaluated using the Molecular Mechanics/Generalized Born Surface Area (MM/GBSA) method. Binding energy profiles for these compounds and their corresponding energy components were estimated using 1000 snapshots from the terminal 50 ns MD trajectories where the systems exhibited conformational stability. This helps minimize the effects of conformational entropy on the energy calculations, which is mathematically expressed as follows:

$$\Delta G_{bind} = G_{complex} - (G_{receptor} + G_{inhibitor}) \quad (1)$$

$$\Delta G_{bind} = \Delta G_{gas} + \Delta G_{sol} - T\Delta S = \Delta H - T\Delta S \quad (2)$$

$$\Delta G_{gas} = \Delta E_{int} + \Delta E_{ele} + \Delta E_{vdW} \quad (3)$$

$$\Delta G_{sol} = \Delta G_{ele,sol(GB)} - \Delta G_{np,sol} \quad (4)$$

$$\Delta G_{np,sol} = \gamma SASA + \beta \quad (5)$$

Accordingly, internal (ΔE_{int}), electrostatic (ΔE_{ele}) and van der Waals (ΔE_{vdW}) energies sum up the gas phase energy (ΔG_{gas}) while the solvation free energy (ΔG_{sol}) is defined by the differential contributions of the polar ($\Delta G_{ele,sol}$) and non-polar ($\Delta G_{np,sol}$) solvation terms. More so, the $\Delta G_{np,sol}$ was solved by estimating the linear relationship between the surface tension proportionality constant (γ = 0.0072 mol^{-1} $Å^{-2}$) and the solvent accessible surface area (SASA, $Å^2$) and a β constant. The MM/GBSA method was used to estimate the Generalized Born (GB) for $\Delta G_{ele,sol}$.

3. Experimental validation methods

3.1. Protein expression and purification

The Human CLIC4 gene was cloned into a pET-28a vector containing an N-terminal hexahistidine tag and a TEV cleavage site. CLIC4 was expressed recombinantly in M9 minimal media supplemented with ^{15}N NH4Cl in the C43 *E.coli* strain (Lucigen). The cells were lysed by sonication, and the membrane and soluble fractions were separated by ultracentrifugation at 117,734 g. The soluble fraction was purified separately in the absence of any detergent using affinity chromatography with Ni IMAC. The elutions were pooled and cleaved with TEV protease, and subsequently, gel filtrated using a Superdex200 Increase column (GE) in either 20 mM HEPES buffer with 20 mM NaCl at pH 7.4.

3.2. Nuclear magnetic resonance (NMR) titrations

The selected high-affinity hit compounds were tested for binding using NMR. Spectra were acquired on a Bruker Avance III

spectrometer at a proton frequency of 600 MHz using a QCIP cryoprobe. ^{15}N TROSY HSQC of ^{15}N labeled CLIC4 were collected in the absence and presence of a two-molar excess of each drug or an equivalent volume of DMSO.

3.3. Culture of human umbilical vein endothelial cells (HUVEC)

HUVECs were purchased from PromoCell and were cultured in endothelial growth medium-2 (Promocell) supplemented with 1% penicillin/streptomycin (Gibco) in 1% gelatin-coated dishes at 37 °C under normoxic conditions (20% O_2, 5% CO_2). The cells were cultured to 70–80% confluence and were treated with 0.003% hydrogen peroxide (H_2O_2), with/without drugs.

3.4. Adenoviral gene transfer

CLIC4 overexpression was induced by adenoviral gene transfer of human CLIC4 (AdCLIC4) while AdTet-off was used as an adenoviral control (AdControl), as previously described [13]. Both were a kind gift from Professor Stuart Yuspa, National Cancer Institute, NIH, Bethesda, USA. Briefly, HUVECs were grown to 80% confluency and were infected with AdControl or AdCLIC4 at a multiplicity of infection (MOI) of 1:100. After 4 h, the media were changed and cells were then incubated upto 24 h at 37 °C, 5% (v/v) CO_2 to induce overexpression (where applicable).

3.5. Immunocytochemistry analysis of CLIC4 membrane translocation

CLIC4 localization within HUVECs was determined by immunocytochemistry analysis based on a previously described protocol [13]. Briefly, HUVECs were cultured in 24-wells on gelatin-coated 13 mm glass coverslips. After 24 h, cells were either untreated or treated with 0.003% hydrogen peroxide (H_2O_2), with/without drugs for 8 h. The cells were then washed with phosphate-buffered saline (PBS), fixed with 4% paraformaldehyde in PBS for 10 min and permeabilised for 10 min with 0.3% Triton X-100 in PBS. Non-specific protein-protein interactions were blocked with incubating the cells in 1% BSA for an hour followed by incubation with anti-CLIC4 antibody (Santa Cruz Biotechnology, clone 356.1, 1/100 dilution) and anti-VE cadherin antibody (Bio-Techne, AF938-SP, 1/500 dilution) overnight at 4 °C. Cells were then washed with PBS and incubated with Alexa Fluor 488 anti-rabbit IgG (green, 1/200 dilution) and Alexa Fluor 488 anti-rabbit IgG (green, 1/200 dilution) for 1 h in the dark. Following a PBS wash step, the cells were mounted with Vectashield Antifade mounting medium with DAPI. All microscopy slides were viewed with a Zeiss LSM-880 confocal microscope using 405 nm, 488 nm, 633 nm lasers. All images were processed with Zen Black and Zen Blue software.

3.6. Wound healing assay to validate endothelial cell responses of drugs

HUVECs were grown to confluency in a 6-well plate and a micro pipettor was used to generate a 1-mm wide scratch on the bottom of the 6-well plate. Cells were then gently washed with PBS and were either untreated or treated with AdControl or AdCLIC4 with/without the drugs for 24 h. Cells were fixed with 4% formaldehyde for 10 min, rinsed and stained with 3% Giemsa. Microscopy was used to observe and photograph cell migration to the scratch area and estimate the effects of drugs on wound healing.

3.7. Cell survival studies

60% confluent HPAECs grown in Corning® 96 well special optics plates were left untreated or were infected with adenoviruses AdCLIC4 and cultured in full medium for 24 hr, with/without drugs [13]. The cells were then incubated with MitoProbe™ DiOC2 (Life Technologies, Invitrogen,USA) for 45 min. DiOC2 penetrates the cytosol of eukaryotic cells and accumulates primarily in mitochondria with active membrane potentials, producing bright, red fluorescence. Images were taken under the under the Olympus IX70 inverted fluorescent microscope and F-view Soft Imaging System camera. The intensity of fluorescence corresponding to the number of live cells was measured with Image J.

4. Results

4.1. Combinatorial search algorithms identified two de novo and druggable allosteric sites

Identifying putative allosteric CLIC4 sites (other than the GSH-binding site) for pharmacological targeting was achieved using integrative method that involves multiple site prediction algorithms; SiteMap [39], DeepSite [40], FTMap [41], DogSiteScore [42], and ProBIS [43]. This integrative approach is essential to validate and cross-validate the allosteric and druggable potentials of these sites. Primarily, three sites (Sites 1–3) were predicted by SiteMap and ranked based on their potentials (Fig. 1A and B, Table 1). More so, global pocket descriptors were estimated, which include the cavity size, volume, enclosure, hydrophobicity, and hydrophilicity to define the chemical tractability (druggability) as well as the morphology of the predicted sites. Site 1 has the highest propensity for druggability with SiteScore = 0.865 and Dscore = 0.871 (threshold: SiteScore ≥ 0.8; Dscore > 0.83) but corresponds with the known CLIC4 GSH-binding site located at the N-terminal domain (residues 1→90). The second predicted region is a component of the α-helical C-terminal domain (residues 100→253). More specifically, Site 2 lies around the flexible foot loop region (residues 159→175) and with estimated SiteScore and Dscore of 0.840 and 0.797 respectively. While a Dscore range between 0.83 and 1 have been used to describe druggable pockets, a Dscore of 0.797 places the identified Site 2 within the Dscore range of 0.7–0.8 used to describe intermediately druggable pockets [48]. Morphologically, Site 2 constitute a flexible loop region that connects the N-terminal domain to the α-helical C-terminal domain. Site 3, which is located adjacent to the GSH binding site has relatively low cavity size (72 A^2), volume (140.973 A^3) and hydrophobicity (0.029) which correlates with lower SiteScore and Dscore of 0.710 and 0.671 respectively, although with a tendency for druggability (intermediate), as predicted by the DogSiteScore algorithm.

As estimated, Site 3 has the highest surface exposure (0.753) as compared to Site 1 (0.739) and Site 2 (0.580) with an enclosure 0.650 for a less well-defined cavity. Functionally, Site 3 residues are located within the α-helical C-terminal domain (residues 100→253) and more specifically proximal to the nuclear localization sequence (NLS, residues 199–206).

Cross-validative predictions to further support the potentials of these predicted pockets were carried out using DogSiteScore, FTMap, DeepSite, and ProBIS (Table 2). Site 1 was commonly predicted across all the four algorithms while two (FTMap and DogSiteScore) complementarily identified residues that constitute Site 2. Moreover, DogSiteScore, PROBIS and DeepSite mapped regions that correlated with the primarily identified Site 3. Druggability estimation (threshold > 0.5) by DogSiteScore further revealed a DrugScoreG of 0.6 (Site 1), 0.53 (Site 2) and 0.78 (Site 3).

4.2. In silico screening and site-directed energy-based sorting led to the selection of site-specific high-affinity hit compounds

This experiment was executed on a HPC-integrated Autodock Vina and entailed a blind screening approach aimed at identifying specific hits (from the 1615 FDA approved compound library) that bind allosterically to the target protein based on preferentiality.

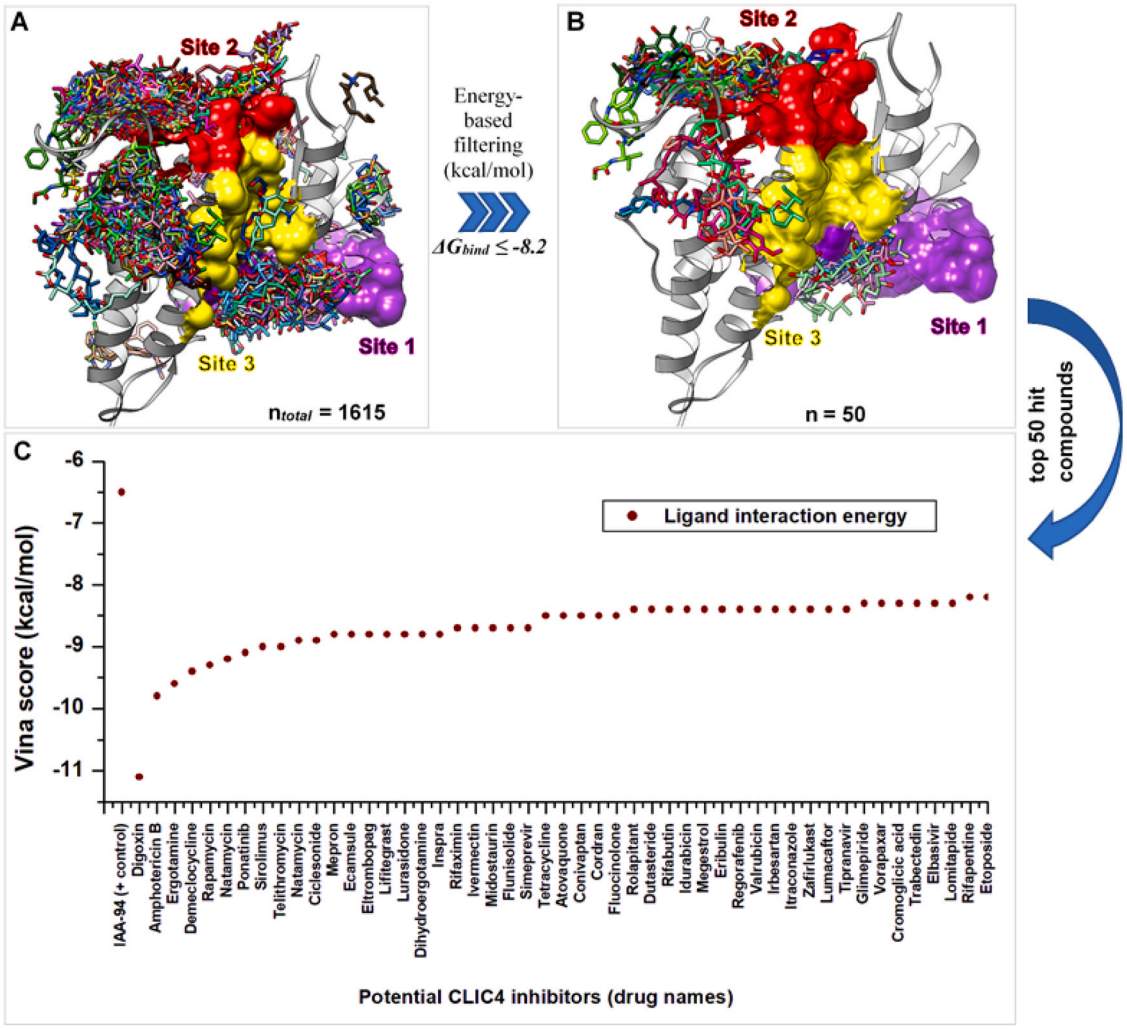

Fig. 1. 3D pocket localization of the predicted Sites 1–3 and blind-docking/screening and selection of potential hit compounds. [A] Blind docking results showing all 1615 FDA compounds binding across various CLIC4 cavities, including the predicted Site 1 (magenta), Site 2 (red) and Site 3 (yellow) all shown in surface representation [B] Energy filtering results of the top 50 hit compounds binding to their preferred target sites on CLIC4. [C] Plot showing the interaction energies of the respective compounds in the top 50 set.

Results were further analyzed based on agreement with allosteric sites prediction earlier performed. Across all the 1615 compound set, energy scores ranged from − 2.3 kcal/mol (lowest affinity → ZINC8034121: cysteamine) to − 11.1 kcal/mol (highest affinity → ZINC242548690: digoxin). An *in-house* filtering algorithm was used to sort compounds with non-GSH site (Site 1) binding activities and interaction energy (ΔG_{bind}) ≤ −8.0 kcal/mol.

Based on energy scoring, results for the top 50 potential CLIC4 inhibitors, including the control compound, IAA94, were curated and presented in Supplementary Table 1. The screened compounds exhibited high diversities in their inhibitory mechanisms against CLIC4 by binding to different cavities based on their complementary interaction affinity (Fig. 1A and B). However, most of the top 50 hit compounds exhibited selective binding to the Site 2 region with variations in their binding energy values (Fig. 1). As estimated, the docking score of IAA94 was − 6.4 kcal/mol and it showed a much lower affinity compared to the top 10 hits with scores between − 8.8 to − 11.1 kcal/mol. The compound with the most inhibitory potential (based on energy scoring) is digoxin ((ΔG_{bind}) = −11.1 kcal/mol) which binds at the predicted Site 2, proximal to the FFL. Structural (visual) analysis revealed hydrogen bonds with Met184 and Ile163, electrostatic interaction (attractive charge) with Asp161, hydrophobic interactions with Pro158, Leu159, Lys172, Ile163, Lys110, Leu105 and Leu107. Unfavorable interactions however occurred with Arg176 and Glu183. Binding regions and modes for other selected top hits are presented in Table 3 and Fig. 2 (0–10). More so, asides amphotericin B (AMPhB) which binds proximally to the predicted Site 3, other hit compounds (from the top 10 subset) majorly exhibited binding at Site 2 with extended interactions into the flexible foot loop region: Ergotamine binds at the predicted Site 2 and exhibited a binding pattern similar to digoxin by extending into the FFL.

Demeclocycline also binds at Site 2 more specifically at the interface of the FFL. Rapamycin (RAPA) binds around the predicted Site 2, making contact with some residues of the FFL and Site 3 to bind stably.

Natamycin extends more into the FFL at the interface with the Site 2 region. Ponatinib binds similar to ergotamine and traverses the Site 2 into the FFL. Telithromycin binds to the Site 2 region and extends into the flexible foot loop as well, a binding pattern similar for Ciclesonide and Mepron. On the contrary, visualizations revealed that IAA94 displayed binding around the predicted Site 1 region which corresponds to the GSH binding domain. Hydrogen bonds were observed with Val54 while hydrophobic interactions were observed with Ile32, Phe42, Trp46, Phe52, and Val54.

For experimental testing, AMPhB and RAPA were selected in addition to the control compound, IAA94 (Fig. 3), firstly, due to their unique binding positioning among the top 10 compound set. According to our findings, both ligands were uniquely binding away

Table 1
SiteMap identification of potential druggable sites on CLIC4 and characterization.

Predicted sites	Residues	Druggability score (Dscore)	SiteScore	Surface-exposure	Pocket Size	Pocket Volume (A^3)	Enclosure	Hydrophobicity	Hydrophilicity	Hydrogen donor/ acceptor
Site 1	24, 25, 26, 27, 33, 34, 35, 36, 37, 57, 59, 61, 62, 63, 64, 65, 69, 70, 71, 72, 73, 74, 75, 122, 197, 239, 242, 243, 244	0.871	0.865	0.739	72	235.641	0.634	0.242	0.941	0.941
Site 2	47, 105, 106, 107, 108, 109, 110, 111, 159, 177, 178, 180, 181, 182, 183, 184, 185, 227	0.797	0.840	0.580	74	141.316	0.610	0.235	1.252	0.797
Site 3	40, 89, 92, 108, 109, 112, 114, 115, 116, 117, 118, 119, 121, 122, 123, 179, 186, 187, 190, 191, 194	0.671	0.710	0.753	42	140.973	0.650	0.029	1.244	0.671

Table 2
Cross-validation of primarily identified druggable sites using multiple prediction methods.

Predicted sites	Potential ligand-binding cavities and cross-validation					Corresponding functional CLIC4 domain
	SiteMap	FTMap	DogSiteScore	PROBIS	DeepSite	
Site 1	24, 25, 26, 27, 33, 34, 35, 36, 37, 57, 59, 61, 62, 63, 64, 65, 69, 70, 71, 72, 73, 74, 75, 122, 197, 239, 242, 243, 244	37, 74, 75, 76, 86, 87, 88, 89	24, 25, 29, 30, 55, 56, 57, 58, 59, 61, 62, 63, 64, 65, 66, 69, 70, 71, 72, 73, 74, 75	24, 34, 35, 36, 37, 74, 75, 76, 87, 88, 89	24, 35–37, 122, 130, 197, 240, 243, 244, 247	N-terminal domain (residues 1–90) *GSH-binding site* [24,34,35,37,38,75,76,87,88,89]
Site 2	47, 105, 106, 107, 108, 109, 110, 111, 159, 177, 178, 180, 181, 182, 183, 184, 185, 227	42, 45, 46, 47, 49, 50, 51, 52, 92, 105, 107, 114, 115, 183, 184, 186, 187, 190, 227	47, 105, 106, 107, 108, 109, 110, 178, 180, 181, 182, 183, 184, 185, 227	–	–	α-helical C-terminal domain (residues 100–253) *flexible foot loop [Leu159 to Thr175]*
Site 3	40, 89, 92, 108, 109, 112, 114, 115, 116, 117, 118, 119, 121, 122, 123, 179, 186, 187, 190, 191, 194	————	40, 92, 109, 114, 115, 116, 117, 118, 119, 120, 121, 122, 148, 149, 150, 151, 179, 186, 187, 190, 191, 192, 194, 195, 196, 198, 199, 208, 210, 217, 218, 221, 225, 230	37, 114, 115, 116, 117, 118, 119, 122, 179, 187, 188, 190, 191, 192, 193, 194, 195	173, 174, 175, 186, 187, 215, 218, 219, 220, 221, 222, 223	*Nuclear localization sequence (NLS) [residues 199–206]*

Table 3
Detailing docking results of the top 10 hit compounds.

S/N	Compound ID (ZINC)	Drug name	Docking score (kcal/mol)	CLIC4 'blind' docking site	Binding modes			
					Hydrogen interactions	Attractive charge interactions	Hydrophobic interactions	Unfavorable interactions
0	–	**IAA94**	**-6.5**	Site 1 [GSH-binding site]	V54	–	I32 F42, W46 F52, V54	–
1	ZINC000242548690	Digoxin	-11.1	Site 2 → flexible foot loop	M184 I163	D161	P158, L159, K172, I163, K110, L105, L107	R176 E183
2	ZINC000253387843	AMPhB	-9.8	Site 3	N89, M119, K194, A123,	–	V247, A123	K194
3	ZINC000052955754	Ergotamine	-9.6	Site 2 → flexible foot loop	T175, S174, L159, L183	–	K110, P158, K172	–
4	ZINC000100036924	Demeclocycline	-9.4	Site 2 → flexible foot loop	N182, R176, T175, G181, P160, L159, D161, P158,	–	I163, P158, K172,	N182
5	ZINC000096006018	Rapamycin	-9.3	Site 2 → flexible foot loop → Site 3	P158, K150	–	I163, I171, P160, Y154	–
6	ZINC000008220909	Natamycin	-9.2	Site 2 → flexible foot loop	E162, D161, S174	D180, E183	–	–
7	ZINC000036701290	Ponatinib	-9.1	Site 2 → flexible foot loop	P109, K110, D180, R176	K110	K110, L159, P158, R176	K106, K110
8	ZINC000009574770	Telithromycin	-9.0	Site 2 → flexible foot loop	E169, P158, R176, S174, D180, T175	E169, D180	I163, P158, K110	K110
9	ZINC000003915154	Ciclesonide	-8.9	Site 2 → flexible foot loop	T175, R176, N182, L159	–	R176, K172, P158, L159	T175
10	ZINC000100017856	Mepron	-8.8	Site 2 → flexible foot loop	T175	–	K110, K172, R176	–

from the catalytic (GSH-binding) site and the predicted Site 2 region (unlike other hits).

Secondly, when the same compound library was screened against other CLICs using the same pipeline, a proportion of the detected FDA approved drugs (including digoxin) also docked with high affinity to other proteins (data not shown)., rendering it not specific to CLIC4. Thirdly, their pharmacological relevance was considered over other compounds in the top 5, particularly with regards to therapeutic usage. For instance, Digoxin is used for treating cardiovascular, however, its long term usage has been associated with incidences of life-threatening conditions like heart attack [49], hence was not selected for further in vitro evaluation.

4.3. AMPhB and RAPA exhibits direct CLIC4 binding and induced significant structural changes

^{15}N–^{1}H HSQC NMR spectra are widely used to monitor protein-small molecule interaction due to their sensitivity to changes in the chemical environment of individual amino acids. To validate the binding of RAPA and AMPhB to CLIC4, we monitored the changes in ^{1}H–^{15}N NMR resonances of CLIC4 in the presence and absence of these drugs, and compared it to the effect of the non-selective chloride channel inhibitor IAA94.

Upon addition of 2 molar excess of AMPhB, significant chemical shift changes were observed for a subset of CLIC4 resonances (Fig. 4). RAPA could only be added to an approximate 0.2 molar excess due to its low solubility in aqueous solution, but still induced moderate changes in the NMR spectra. IAA94, on the other hand, failed to induce any significant chemical shift changes in CLIC4 spectra, indicating that IAA94 cannot bind to CLIC4 in its soluble state. An example of a higher affinity of AMPHb to CLIC4 is demonstrated in an additional saturation transfer difference NMR data collected (Supplementary Fig. 1).

4.4. AMPhB and RAPA inhibits CLIC4 membrane translocation and ameliorates oxidative stress in endothelial cells

Levels of CLIC4 are known to increase under cellular stress conditions such as oxidative stress in a variety of cells [50]. We have previously shown that oxidative stress promotes significantly higher expression of CLIC4 in HPAECS resulting in endothelial dysfunction [13]. This was accompanied by deleterious endothelial responses including an increase in VEGF mediated angiogenesis [13]. Here, we investigated the inhibitory properties of AMPhB and RAPA on the deleterious effects of CLIC4 on HUVECs.

Under normal condition, CLIC4 is modestly expressed or mostly limited to cell cytosol. HUVECs treated with hydrogen peroxide induces oxidative stress and significantly increased CLIC4 levels in all cellular compartments including plasma membrane. These effects were partly reversed by the addition of AMPhB and RAPA, indicating inhibition of CLIC4 response to oxidative stress induced by peroxides (Fig. 5, A-D).

Cell migration is a key indicator of many biological processes including inflammation, angiogenesis and cancer progression [51]. Widely known in vitro cell migration assay method (wound healing assay) were used to examine the effect of AMPhB and RAPA on HUVECs with adenoviral overexpression of CLIC4 as a positive control to promote cell migration (as has been previously shown [17]). All treatments have no significant effects on cell viability apart from CLIC4 overexpression (Supplementary Fig. 2) that are known to promote cell number and viability for angiogenesis to occur [17]. AMPhB and RAPA treatment attenuated cell migration promoted by CLIC4 (Fig. 5 E-H) which confirms its anticipated anti-migratory effects on endothelial cells.

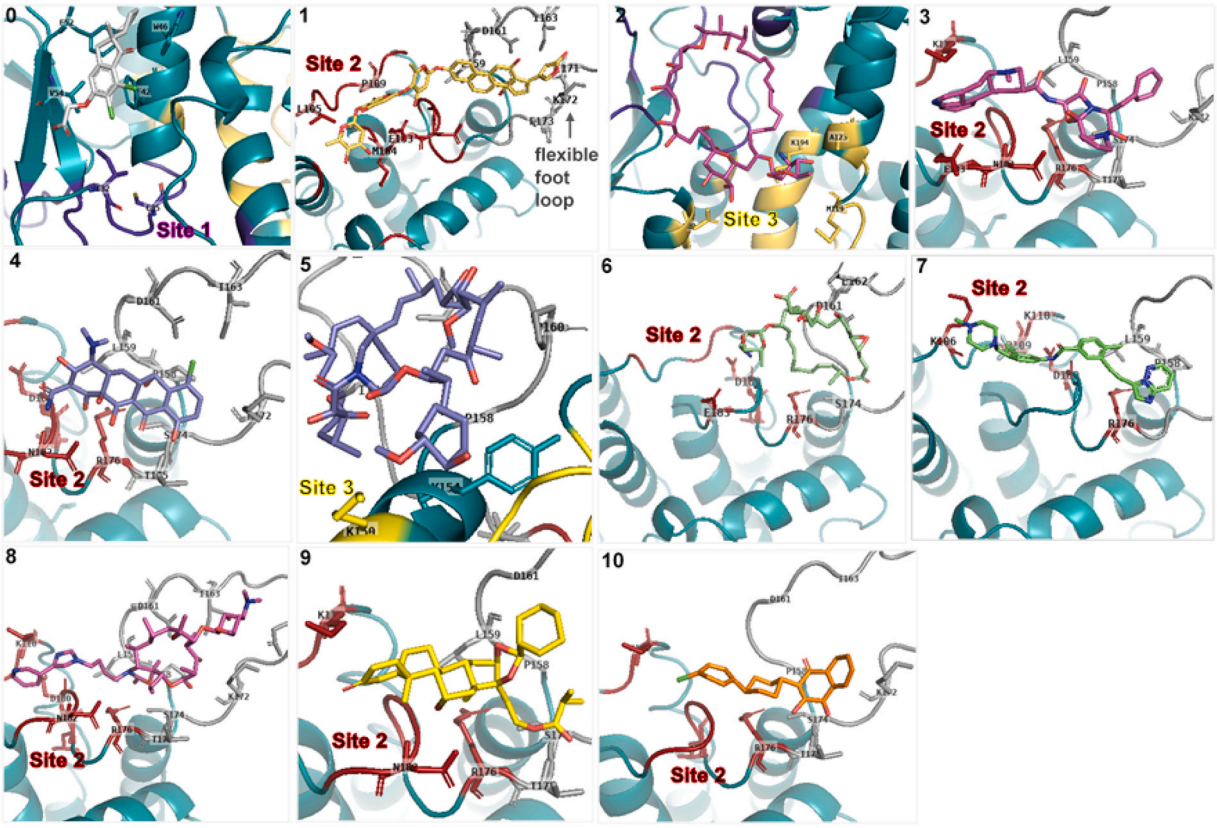

Fig. 2. Binding modes and target sites of top 10 potential inhibitors of CLIC4. 0. IAA94 1. Digoxin 2. AMPhB 3. Ergotamine 4. Demeclocycline 5. RAPA6. Natamycin 7. Ponatinib 8. Telithromycin 9. Ciclesonide 10. Mepron.

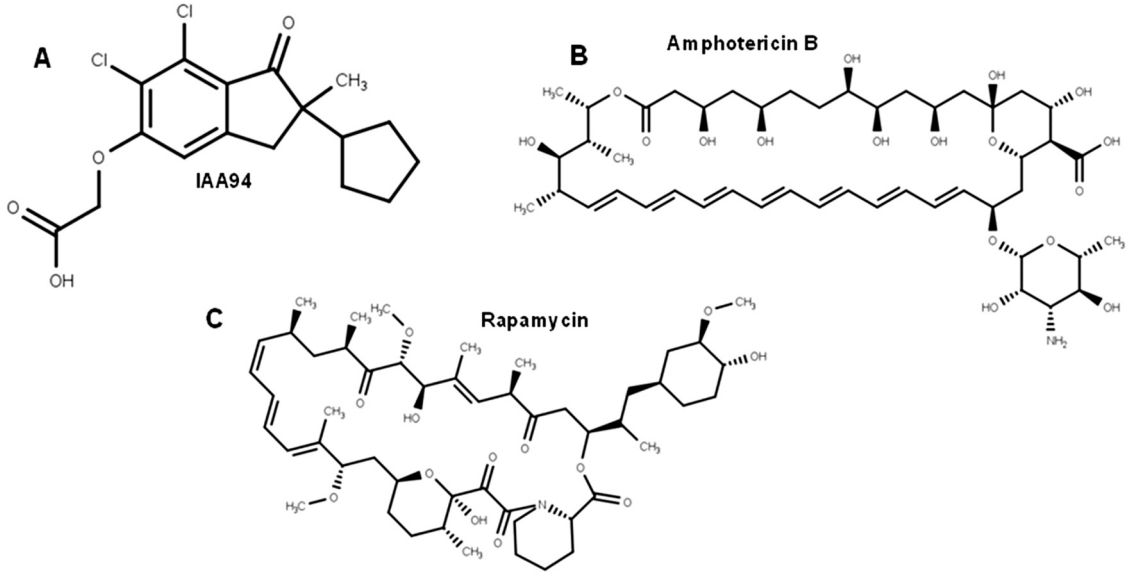

Fig. 3. 2D structures of potential CLIC4 inhibitors. A. IAA94 (control) B. AMPhB and C. Rapamycin.

4.5. Site-specific binding of AMPhB and RAPA induced characteristic changes in CLIC4 structure and dynamics

Conformational events associated with the targeted binding of these inhibitor compounds to the protein were evaluated using an all-atom MD simulation approach. This was important to understand structural changes with respect to AMPhB and RAPA binding, as validated in vitro.

Firstly, the stability of the whole protein systems across the entire simulation time-frames relative to changes in Cα atomistic motions were measured using the Cα-root mean square deviation (RMSD). As estimated, unbound CLIC4 (APO) exhibited a very high degree of structural instability until ~375 ns time-frame where it attained convergence with lowered deviations (Fig. 6). Relatively, RAPA and AMPhB notably lowered the RMSD by ~2 Å indicative of their stabilizing effects on the protein. Corresponding mean RMSD values are shown accordingly in Supplementary Table 2. Stable trajectories from the last 50 ns (450–500 ns) of the MD simulations were retrieved for all systems and used for subsequent global

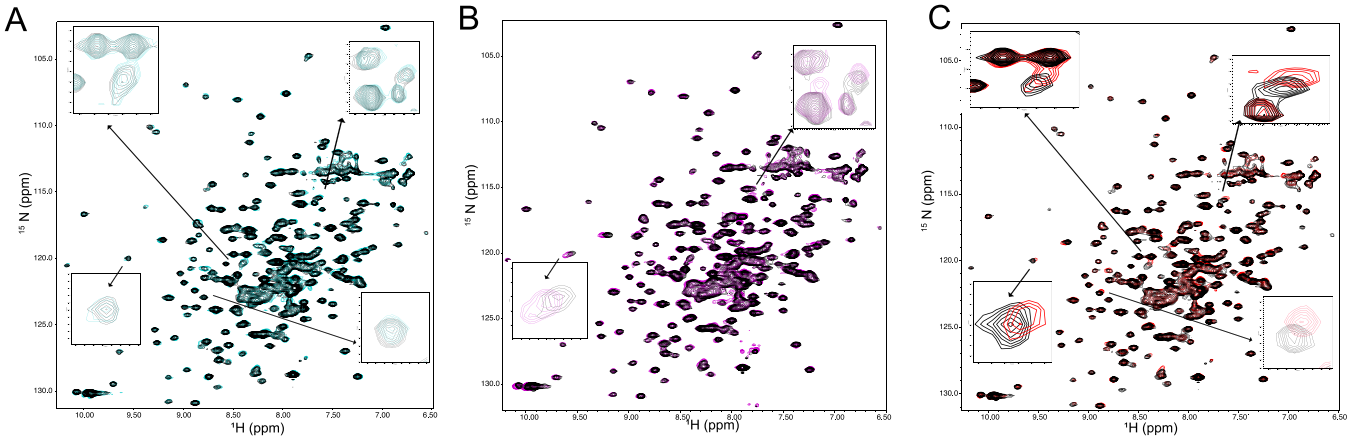

Fig. 4. Binding of AMPhB and RAPA to CLIC4. ^{1}H–^{15}N TROSY HSQC spectra of CLIC4 in the absence (black) and presence of two molar excess of IAA94 (A, cyan), RAPA (B, magenta) and AMPhB (C, red). Regions showing significant chemical shift changes upon addition of RAPA and AMPhB are expanded and compared to similar regions in the IAA94-bound spectrum.

analyses to provide a smaller deviation. RMSD distribution violin plots were employed to measure variations in CLIC4 conformation in the presence and absence of the compounds.

As shown in Fig. 6D, unbound CLIC4 exhibited bimodal conformational distributions which indicates multiple conformations attained over the course of the simulation. Unimodal distributions were however observed in AMPhB- and RAPA-bound CLIC4 indicative of their roles in stabilizing the protein structure. The effects of the compounds on the compactness of the whole protein was further investigated using radius of gyration (RoG) calculations. From the plots (equilibrated timeframes), the binding of AMPhB and RAPA resulted in an increased protein RoG ($_{AMPhB}$Mean_RoG (Å) = 19.83 ± 0.12; $_{RAPA}$Mean_RoG (Å) = 20.56 ± 0.12) which correlates with the loss in structural compactness relative to the unbound protein ($_{APO}$Mean_RoG (Å) = 19.36 ± 0.10).

Furthermore, changes in residual fluctuations within the protein with respect to ligand binding were monitored using Cα-root mean square fluctuation (RMSF) metrics and shown in Fig. 7B and D. As observed, notable fluctuations occurred around residues 54–75 and 159–175 which, respectively, mapped out to the connecting loop (CL) and FFL regions of the protein. However, the intensity of fluctuation was highest in the presence of IAA94. Peculiar to the binding of RAPA are fluctuations of residues 25–34, which constitute the catalytic (GSH-binding) loop (catL$_{GSH}$) while the binding of AMPhB specifically induced the flexibility of residues 80–84 that form an extended β-sheet loop (catL$_{β}$) from the GSH-binding site.

Corresponding mean RMSF values for these structural elements are presented in Table 4. To corroborate these ligand-binding effects, the relative C-α stability and compactness were evaluated using the RMSD and RoG distributions (Fig. 8A-E). Relative to other systems,

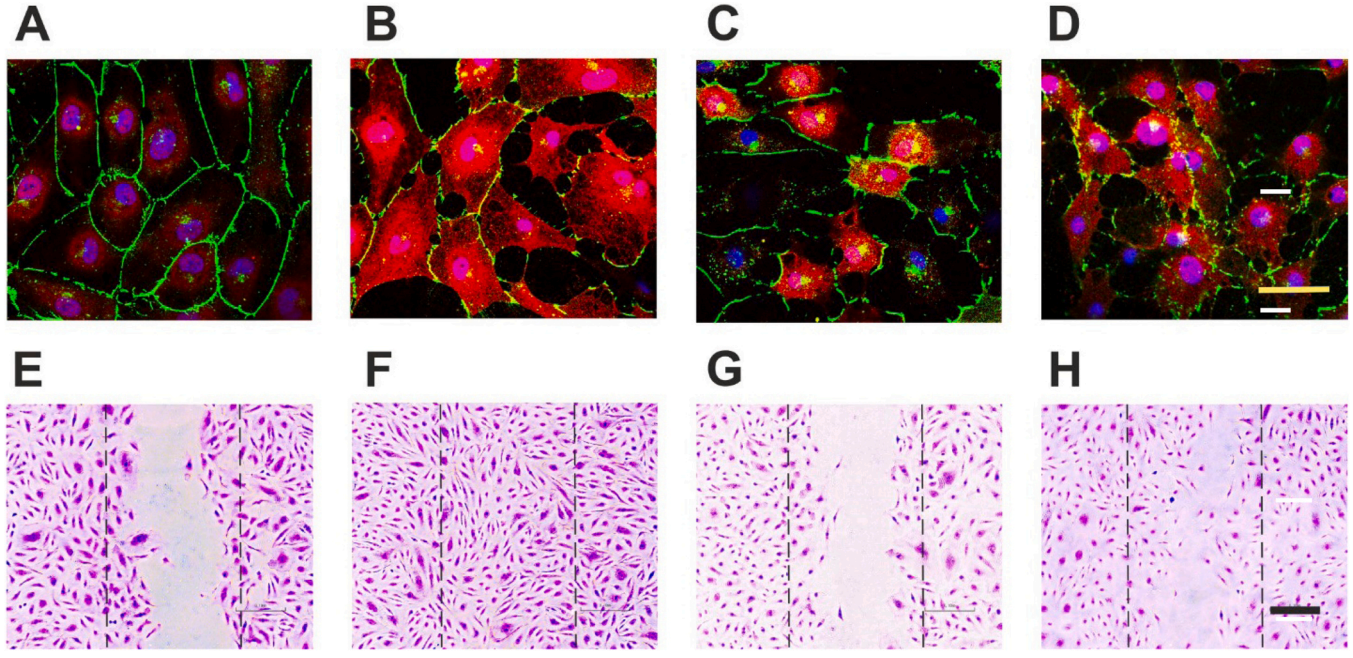

Fig. 5. AMPhB and RAPA inhibits CLIC4 membrane translocation and endothelial cell migration. Top Panel: (A) HUVECs (Control) immunostained for CLIC4 (red), VE-cadherin (cell junctions, green) and DAPI (nucleus, blue) under confluent conditions show the presence of CLIC4 within cytosol and nucleus with the maintenance of endothelial cell barrier indicated by the tight cell-cell junctions. (B) HUVECs treated with 0.003% hydrogen peroxide (H_2O_2) significantly increased the expression levels of CLIC4, including at the plasma membrane with disruption to the barrier functions. These effects were partially reversed when treated with (C)10 μM AMPhB or (D) 10 μM RAPA as indicated by decreased CLIC4 staining in the cells, especially at the plasma membrane. Scale bar = 200 μM. Bottom Panel Representative images of HUVECs "scratch-wounded" using a universal 10 μl pipette tip (scratched area indicated by the broken lines) that are treated with (E) control adenovirus (AdControl) or (F) adenovirus to overexpress CLIC4 (AdCLIC4) alone or with (G) 10 μM AMPhB or (F) 10 μM RAPA. Migration pattern of cells into the 'scratch-wounded' area indicate that both drugs attenuated AdCLIC4- induced cell migration. Scale bar = 100 μM.

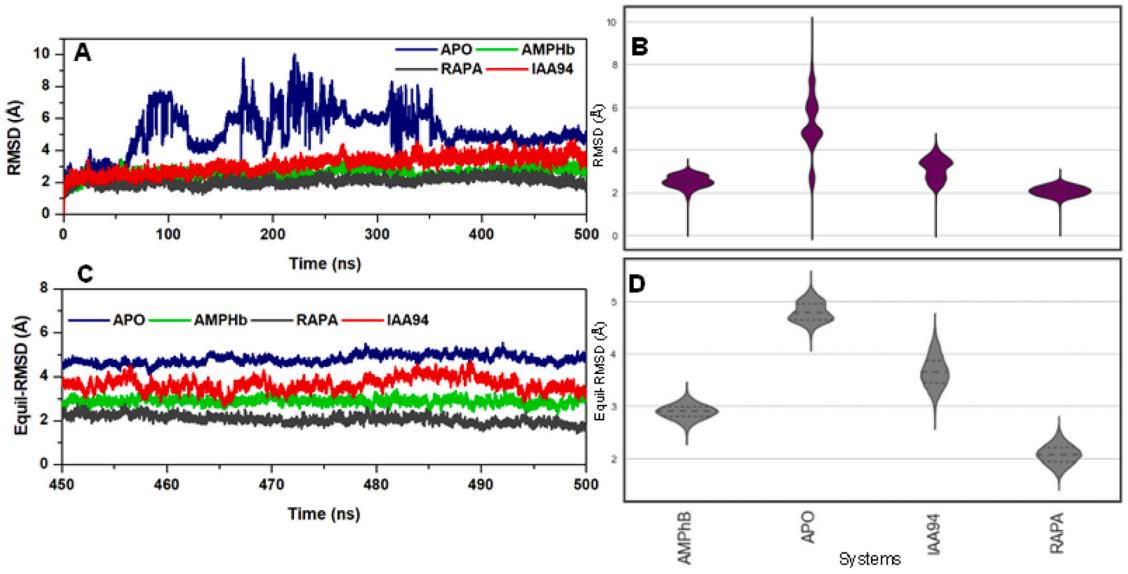

Fig. 6. RMSD plots for unbound and ligand-bound CLIC4. [A] Whole time-frame (500 ns) RMSD plot showing high deviations in unbound CLIC4 relative to stable ligand-bound systems. [B] RMSD distribution density plots for whole time RMSD. [C] Final equilibrated RMSD plots obtained from the terminal 50 ns [D] RMSD distribution density plots for final equilibrated RMSD.

RAPA allosteric induced a bimodal distribution at the $catL_{GSH}$indicative of its distortive effect. More so, the binding of AMPhB caused a notable conformational alteration at the $catL_{\beta}$with a corresponding increase in Cα motions (Fig. 8C). These loops distinctly impacted by RAPA and AMPhB are proximal to the GSH site and when distorted possibly interferes with the GSH-dependent activity of CLIC4 which is crucial to their cellular catalytic roles.

This could underlie their inhibitory mechanisms. 3D representations of the degree of structural alteration at these regions are shown in Fig. 8D-F. It is also important to mention that although none of the compounds elicited effects at the connecting N-C terminal loop (NC_{loop}; residues 100–113), their effects were varied on the proximal FFL (Fig. 8E). As seen, while high distortions characterized the loop in unbound and IAA94 systems, it appeared to be more stable in CLIC4 bound by AMPhB and RAPA. This could as well impact on the mobility of the protein as this region is crucial for CLIC4 translocation from the cytoplasm to the membrane.

Table 4
Mean FE-RMSF calculations for important CLIC4 structural elements.

Residual fluctuation (Å)				
Structural elements	CLIC4	CLIC4 +control	CLIC4 +AMPhB	CLIC4 +RAPA
CL	1.41 ± 0.58	1.81 ± 1.05	1.25 ± 0.37	1.29 ± 0.57
$catL_{GSH}$	1.35 ± 0.29	1.42 ± 0.29	1.31 ± 0.17	1.68 ± 0.68
FFL	2.01 ± 0.78	2.31 ± 1.12	1.79 ± 0.80	1.62 ± 0.83
NC_{loop}	0.89 ± 0.30	0.99 ± 0.30	0.88 ± 0.31	0.87 ± 0.24
$catL_{\beta}$	0.98 ± 0.29	1.24 ± 0.66	1.93 ± 0.43	0.96 ± 0.27

Similarly, the connecting loop region exhibited a more stable conformations in the presence of AMPhB and RAPA but showed bimodal RMSD distributions in unbound and IAA94-bound CLIC4 (Fig. 8B).

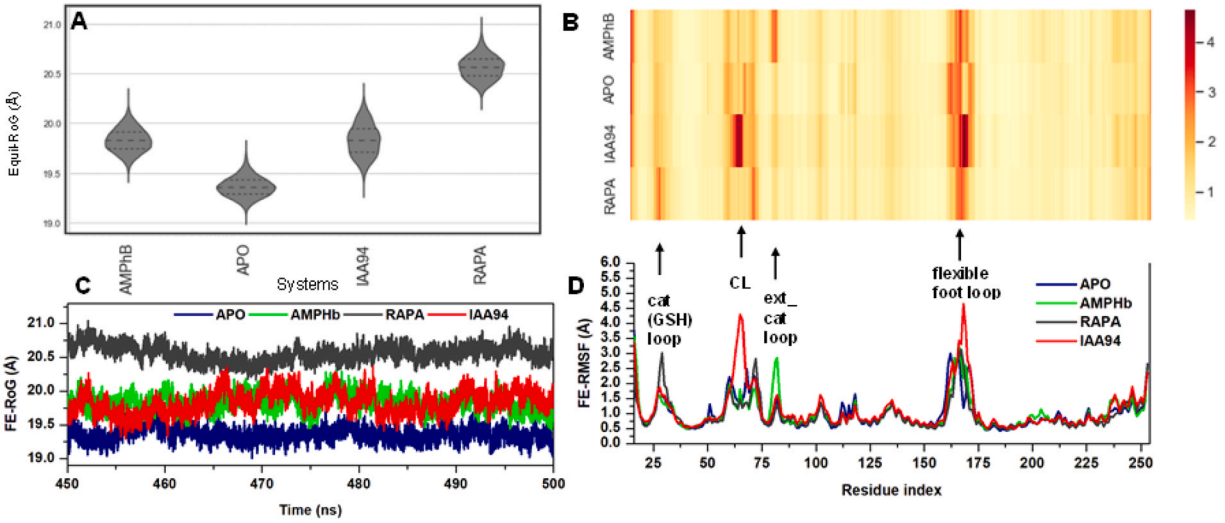

Fig. 7. RoG and RMSF plots measuring variations in structural compactness and residual fluctuations [A] Density distribution plots of equilibrated RoGs [B] Heatmap showing fluctuations among of constituent residues [C] equilibrated RoG line plots [D] RMSF line plot mapping out corresponding residues and their degree of fluctuations as indicated in B.

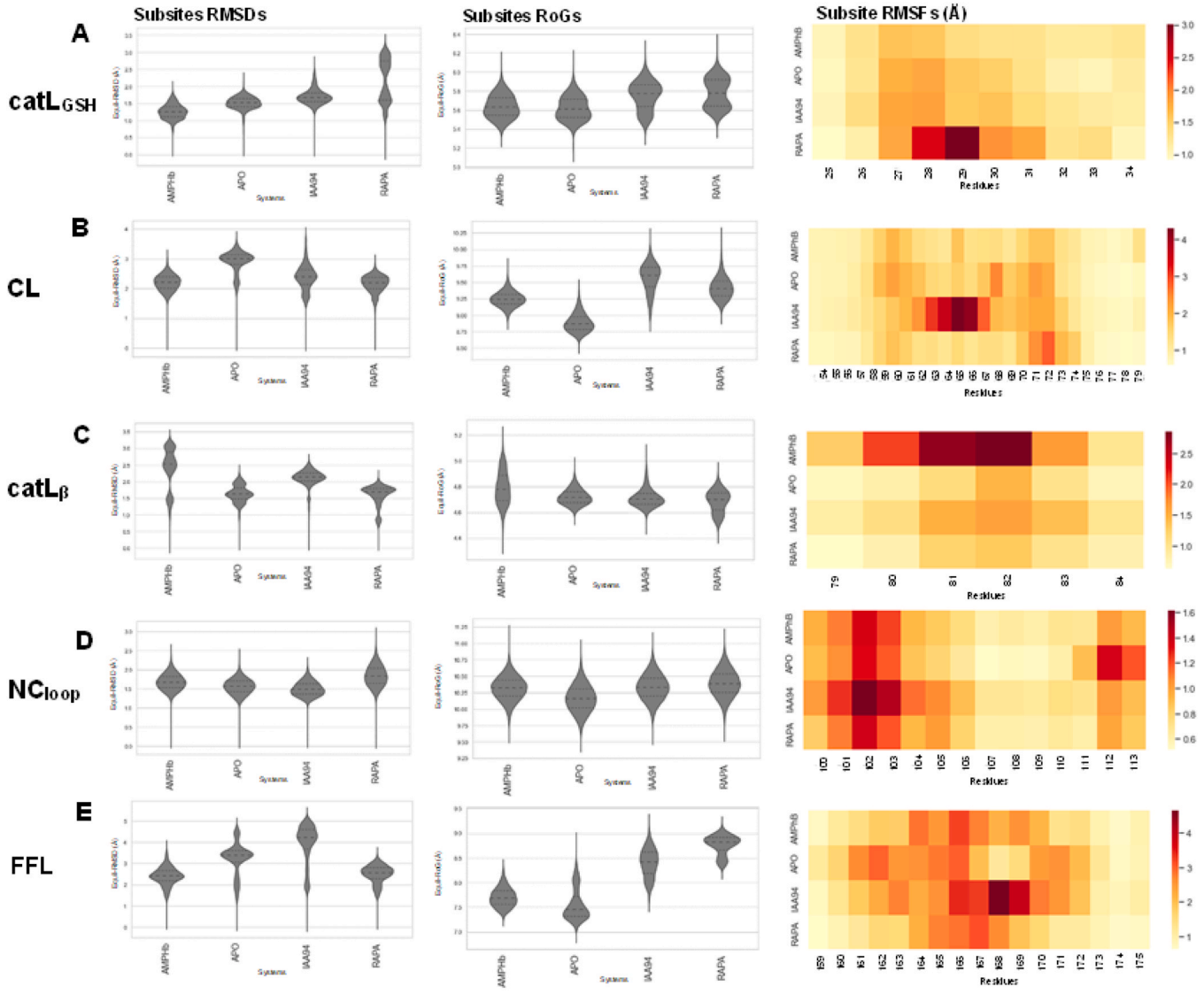

Fig. 8. Conformational RMSD, RoG and RMSF analyses for important subsites on CLCI4 with notable ligand effects [A] proximal catalytic (GSH) loop [B] connecting loop [C] extended catalytic loop [D] N-to-C terminal connecting loop [E] flexible foot loop.

Table 5
Binding free energy profiles of AMPHb, RAPA and IAA94.

Energy components (kcal mol^{-1})	CLIC4+AMPhB	CLIC4+RAPA	CLIC4+IAA94
Δ*E*vdW	− 48.0 ± 0.3	-33.4 ± 1	-24.1 ± 0.2
Δ*E*ele	-160.0 ± 2.4	-14.7 ± 0.4	-10.0 ± 0.3
Δ*G*gas	-208.0 ± 2.5	-48.0 ± 1.0	-34.0 ± 0.3
Δ*G*ele,sol(GB)	174.3 ± 2.1	29.2 ± 0.6	14.8 ± 0.3
Δ*G*np,sol	-7.6 ± 0.1	-4.3 ± 0.1	-3.2 ± 0.02
Δ*G*sol	166.7 ± 2.0	24.9 ± 0.6	14.8 ± 0.3
-*T*Δ*S*	*0.0*	*0.0*	*0.0*
ΔG_{bind}	-41.4 ± 0.6	-23.1 ± 0.5	-19.2 ± 0.2

4.6. MM/GBSA calculations revealed mechanistic variations in the relative binding affinities of AMPhB and RAPA to CLIC4

The respective affinities (binding free energies, ΔG_{bind}) by which the inhibitors bind to CLIC4 were determined using the MM/GBSA method which also provided insights into the contributions of the various energy components to achieve ligands' stable binding. This also was used as an approach to validate the initially derived docking affinities. It is important to further emphasize that the final equilibrated (stable) time-frames (last 50 ns) were employed for the energy calculations in order to minimize deviations. From our calculations, AMPhB exhibited the most favorable ΔG_{bind} of − 41.4 kcal/mol while RAPA had a ΔG_{bind} value of − 23.1 kcal/mol. Relatively, IAA94 had the least binding affinity with an energy value of − 19.2 kcal/mol (Table 5). As observed, these findings also correlate with the order of the binding (Vina) scores.

More so, electrostatic energies (**Δ*E*ele**) had the most contributions to the stable binding of AMPhB at Site 3 while van der Waals (**Δ*E*vdW**) was most prominent to RAPA and IAA94 at their respective allosteric binding sites. Using the average structures, 2D mapping of the ligand-residue interactions further revealed the involvement of the terminal aminium group of AMPhB to form strong N–O (strong attractive charge-charge bonds) with E93 and a NH–O salt-salt bridge with E92 (Fig. 9A). Also involved in interacting with the aminium group is N190 via conventional NH–O while the oxane moieties interacted via additional hydrogen (NH–O and CH—O) bonds with D87, N89, and K90. These strong interactions corroborate the high **Δ*E*ele** values estimated which collectively, could further support the ligand-binding stability. Also, π (aromatic) interactions observed with M119, A243 and Y244 contribute towards the **Δ*E*vdW** which also impacts on ligand stability. A high Δ*G*ele,sol(GB) and

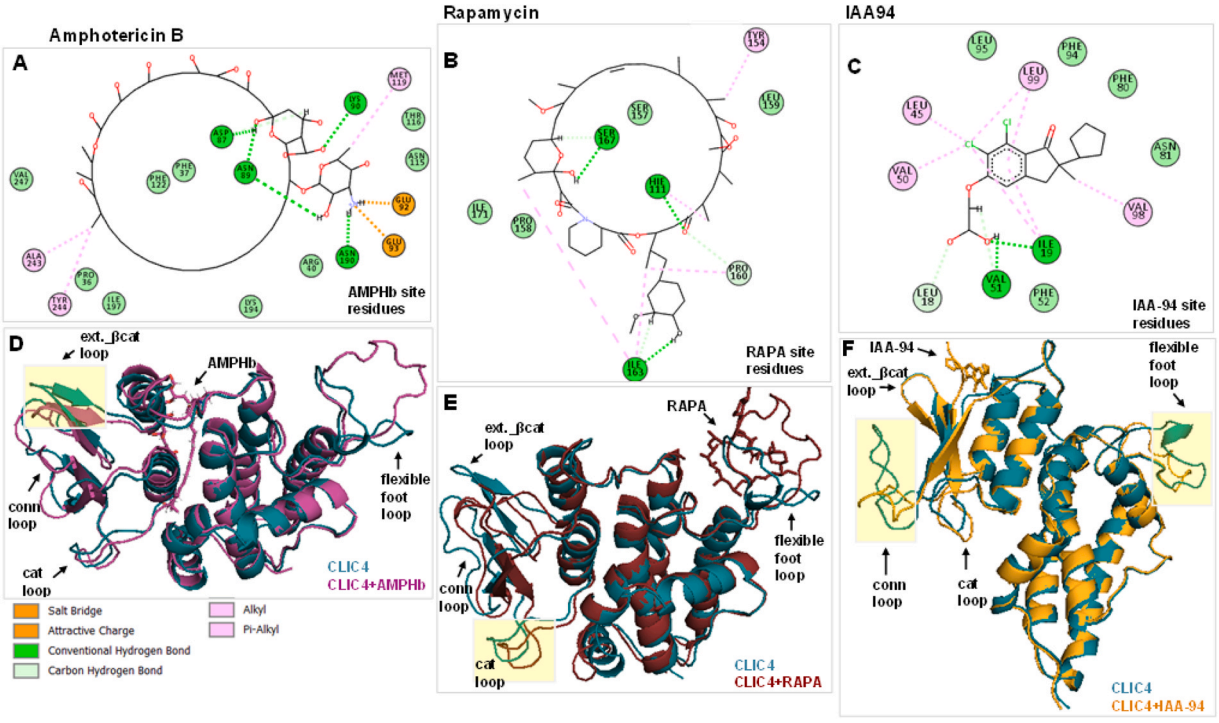

Fig. 9. 2D mapping of residue interactions. Residue mapping for [A] CLIC4 and AMPhB [B] CLIC4 and RAPA[C] CLIC4 and IAA94. 3D superposition of unbound and [D] AMPhB [B] RAPA[E] IAA94-bound CLIC4 showing alterations at key regions.

ΔGsol for AMPhB indicates its interaction was more favorable within the Site 3 pocket and with constituent residues away from the regions accessible by solvent. This correlates with the estimated non-polar energy (ΔGnp,sol) of − 7.63 kcal/mol which favors the hydrophobic interaction of the inhibitor. Furthermore, π interactions were prominent in the binding of RAPA and involved Y154, P160, I163, H111 which could account for the high ***vdW*** energies. In addition, S167 interacted with the oxane group of RAPA while H111 formed conventional hydrogen (NH–O) with an extending carbonyl group. I163 also interacts with the 1-diol group of the terminal hexanol ring via a conventional NH–O altogether contributing to the binding stability of RAPA (Fig. 9B). RAPA exhibited a favorable non-polar (hydrophobic) binding (ΔGnp,sol) similar to IAA94 which also had more ***vdW*** energies to attain a stable binding. Prominent to the binding of IAA94 were π interactions involving I19, L45, V50, V98 and L99, while I19 and V51 contributed conventional H-bonds to IAA94 binding (Fig. 9C).

5. Discussion

CLIC4 is not a typical ion channel protein but metamorphic in nature, which accounts for its involvement with numerous downstream pathways and effectors across diverse cell forms and processes. This functionality, however, makes it central to the development of various cancer and vascular diseases, among others. The significance of inhibiting CLIC4 to ameliorate pathologies have been previously reported and involved the use of research methods like gene knockout and RNAi approaches [17,52–54]. Notable is a study by Abdul Salam et al., which showed CLIC4/Arf6 inhibition and ameliorative effects in PAH [18]. However, no specific CLIC4 inhibitor has been identified to date thereby limiting translatable interventions. Here, we used FDA approved compounds with known safety data to identify pharmacological inhibitors that can be repurposed. This potentiates translational research in in diseases affected by CLIC4 where efficacy and dosing can be further scrutinized.

This study incorporates structure-based approaches and for the first time, reports small-molecule inhibitors of CLIC4. We report novel allosteric (non-GSH) sites on the protein which are highly suitable for targeting by chemical compounds or entities. We also demonstrated, experimentally, the potentials of the identified hit compounds to bind to CLIC4 and attenuate CLIC4 mediated cell responses such as translocation to the plasma membrane which is known to be increased in diseased conditions [50,55] and angiogenesis.

The soluble form of CLIC4 is structurally related GST and thought to exhibit GSH-dependent enzymatic activity [56]. This accounted for the use of IAA94, a general chloride channel blocker, as the control compound in this study. Though its CLIC binding property has been widely reported, the specific binding region on CLIC4 remains elusive. Our inhibitor screening study demonstrated that it potentially binds around the GSH binding site which is most likely due to its chemical similarity with ethacrynic acid, a known GST inhibitor. However, its binding affinity is relatively low compared to the hit compounds and our experimental studies corroboratively revealed that IAA94 poorly binds to CLIC4, relative to the hit compounds. From the NMR data, IAA94 failed to induce any significant chemical shift perturbations on the NMR spectrum of CLIC4, indicating its inability to bind CLIC4 in this soluble form. This could also indicate that conformational changes induced by IAA94 as observed in the MD studies have no translatable effects in vitro and that many of the inhibitory effects widely reported in literature may be due to indirect effects or limited to the channel form alone.

The lack of information on possible allosteric (non-GSH) and druggable sites on CLIC4 has not favored previous implementation of structure-based discovery of potential CLIC4 inhibitors. This further explains the significance of this present study and how it aids future research efforts. Identifying allosteric inhibitors is more advantageous in the drug development process as it provides a more feasible avenue to discover drug molecules with high target specificity. This is because, contrary to orthosteric sites, allosteric sites are less conserved, hence drugs binding to these regions are more specific and most likely, less toxic to human [57,58].

Importantly, we identified two high-affinity sites in CLIC4 other than the known GST-like site that is highly conserved among the CLIC protein family. An interesting finding was the identification of the flexible foot loop region (Site 2) and its high potentials for allosteric targeting by small-molecule compounds. Consequentially, a large proportion of the predicted hit compounds interacted preferentially at this region with high affinities. Functionally, the flexible foot loop region is crucial for the membrane translocation of CLIC proteins, and, if effectively inhibited, could prevent CLIC4 cellular motility which is essential for various pathological involvement. This study therefore opens avenues to explore site targetability, particularly, the identification of crucial interactive residues such as P158, L159, Thr175 and Arg176 among others, which will be essential for future site-specific structure-based inhibitor design studies.

Although our predicted inhibitors (AMPhB and RAPA) did not significantly impact on the FFL region, our MD simulation study revealed their respective allosteric effects were more prominent on the catalytic loops. Distortions in key catalytic region of CLIC4 as induced by these proteins could in turn affect its enzymatic activity and to a larger extent, effector protein interactions. Corroboratively, NMR results revealed that both RAPA and AMPhB induced structural changes in CLIC4. While the low water solubility of RAPA makes it impossible to compare affinities, both molecules display clear chemical shift perturbations on a small subset of peaks in the $^{1}H–^{15}N$ NMR spectrum of CLIC4. Additionally, residues involved in high-affinity interactions with inhibitor molecules are essential for binding stability and such residues; Asp87, Asn89, Lys90, Glu92, Glu93 and Asn190 for AMPhB, and His111, Pro160, Ile163, and Ser167 for RAPA could be explored in future studies for discovering ligands with improved specificity for both sites. Interestingly, RAPA is increasingly reported to improve cardiovascular health and treat cancer- implicating the potential involvement of CLIC4 in mediating its effects [59,60] while the role of AMPhB in these disease states is yet to be reported and requires further exploration. Furthermore, the impact of both compounds on CLIC4 enzymatic activity could correlate with their abilities to ameliorate known CLIC4-induced effects on cellular stress and cell migration. *In vitro* validation assay using endothelial cell system further reflects the functional effects of the NMR and MD binding observations and showed that the tested compounds were able to inhibit CLIC4-mediated endothelial response especially in perpetrated pathological conditions. The precise mechanism of this however, needs further investigation but is likely to involve the VEGF, SIP-1 or m-TOR pathways.

In summary, we employed structure-based methods that led to the identification of AMPhB and RAPA as allosteric inhibitors of CLIC4. Experimental validation studies further confirmed their binding potentials and ability to reverse CLIC4-mediated cellular dysfunctions. This presents an important advancement in therapeutic strategies to specifically target the pathological involvement of CLIC proteins.

Funding

This research did not receive any specific grant from funding agencies in the public, commercial, or not-for-profit sectors. Dr Fisayo Olotu is funded by Medicine in Malaria Ventures, Geneva, Switzerland and Dr. Abdul Salam is funded by Barts Charity, UK.

CRediT authorship contribution statement

Fisayo Olotu: Conceptualization, Methodology, Validation, Formal analysis, Investigation, Data curation, Writing – original draft, Writing – review & editing, Visualization. **Encarnacion Medina-Carmona:** Investigation. **Angela Serrano-Sanchez**: Investigation and review. **Felipe Ossa:** Investigation and review. **Abdelaziz El-Hamdaoui:** Investigation. **Özlem Tastan Bishop:** Methodology, Resources, Writing – review & editing. **Jose L. Ortega-Roldan:** Formal analysis, Visualization, Writing – review & editing. **Vahitha B. Abdul-Salam:** Conceptualization, Validation, Formal analysis, Investigation, Writing – review & editing, Visualization, Resources, Supervision, Funding acquisition.

Conflict of interest

None.

Acknowledgment

We would like to thank the Center for High-Performance Computing, Cape Town, South Africa for providing computational resources and Dr Nabil Hajji for his kind contributions in enhancing the staining protocol.

Appendix A. Supporting information

Supplementary data associated with this article can be found in the online version at doi:10.1016/j.csbj.2022.12.040.

References

[1] Hutchings CJ, Colussi P, Clark TG. Ion channels as therapeutic antibody targets. MAbs 2019;11:265–96.
[2] Gururaja Rao S, Ponnalagu D, Patel NJ, Singh H. Three decades of chloride intracellular channel proteins: from organelle to organ physiology 11.21.1-11.21.17 Curr Protoc Pharmacol 2018;80(1). 11.21.1-11.21.17.
[3] Littler DR, et al. The enigma of the CLIC proteins: ion channels, redox proteins, enzymes, scaffolding proteins? FEBS Lett 2010;17(584(10)):2093–101.
[4] Argenzio E, Innocenti M. The chloride intracellular channel protein CLIC4 inhibits filopodium formation induced by constitutively active mutants of formin mDia2. FEBS Lett 2020;594:1750–8.
[5] Argenzio E, Moolenaar WH. Emerging biological roles of Cl- intracellular channel proteins. J Cell Sci 2016. https://doi.org/10.1242/jcs.189795
[6] Dozynkiewicz MA, et al. Rab25 and CLIC3 collaborate to promote integrin recycling from late endosomes/lysosomes and drive cancer progression. Dev Cell 2012;22:131–45.
[7] Khamici HAl, et al. Members of the chloride intracellular ion channel protein family demonstrate glutaredoxin-like enzymatic activity. PLoS One 2015;10:115699.
[8] Shukla A, et al. TGF-beta signalling is regulated by Schnurri-2-dependent nuclear translocation of CLIC4 and consequent stabilization of phospho-Smad2 and 3. Nat Cell Biol 2009;11:777–84.
[9] Argenzio E, et al. Profilin binding couples chloride intracellular channel protein CLIC4 to RhoA-mDia2 signaling and filopodium formation. J Biol Chem 2018;293:19161–76.
[10] Jiang L, et al. CLIC proteins, ezrin, radixin, moesin and the coupling of membranes to the actin cytoskeleton: a smoking gun? Biochim Biophys Acta Biomembr 2014;1838:643–57.
[11] Argenzio E, et al. CLIC4 regulates cell adhesion and β1 integrin trafficking. J Cell Sci 2014;127:5189–203.
[12] Shukla A, et al. CLIC4 regulates TGF-β-dependent myofibroblast differentiation to produce a cancer stroma *2014 337* 33 Oncogene2013:842–50.
[13] Wojciak-Stothard B, et al. Aberrant chloride intracellular channel 4 expression contributes to endothelial dysfunction in pulmonary arterial hypertension. Circulation 2014;29(129(17)):1770–80.
[14] Domingo-Fernández R, Coll RC, Kearney J, Breit S, O'Neill LAJ. The intracellular chloride channel proteins CLIC1 and CLIC4 induce IL-1β transcription and activate the NLRP3 inflammasome. J Biol Chem 2017;292:12077–87.
[15] Gururaja Rao S, Patel NJ, Singh H. Intracellular chloride channels: novel biomarkers in diseases. Front Physiol 2020;11:96.
[16] Peretti M, et al. Chloride channels in cancer: focus on chloride intracellular channel 1 and 4 (CLIC1 AND CLIC4) proteins in tumor development and as novel therapeutic targets. Biochim Biophys Acta Biomembr 2015;1848(10 Pt B):2523–31.
[17] Abdul-Salam VB, et al. CLIC4/Arf6 pathway: a new lead in BMPRII inhibition in pulmonary hypertension. Circ Res 2019;4(124(1)):52–65.
[18] Suh KS, et al. CLIC4 is a tumor suppressor for cutaneous squamous cell cancer. Carcinogenesis 2012;33:986–95.
[19] Chiang PC, Chou RH, Chien HF, Tsai T, Chen CT. Chloride intracellular channel 4 involves in the reduced invasiveness of cancer cells treated by photodynamic therapy. Lasers Surg Med 2013;45:38–47.
[20] Bohman S, et al. Proteomic analysis of vascular endothelial growth factor-induced endothelial cell differentiation reveals a role for chloride intracellular channel 4 (CLIC4) in tubular morphogenesis. J Biol Chem 2005;280:42397–404.

[21] Patel D, Ythier D, Brozzi F, Eizirik DL, Thorens B. Clic4, a novel protein that sensitizes β-cells to apoptosis. Mol Metab 2015;4:253–64.
[22] Littler DR, et al. The enigma of the CLIC proteins: Ion channels, redox proteins, enzymes, scaffolding proteins? FEBS Lett 2010;584:2093–101.
[23] Ponnalagu D, et al. Chloride channel blocker IAA-94 increases myocardial infarction by reducing calcium retention capacity of the cardiac mitochondria. Life Sci 2019;235:116841.
[24] Rao SG, et al. Identification and characterization of a bacterial homolog of chloride intracellular channel (CLIC) protein (1):85002017. Sci. Rep 2017;7(17):7. (1):85002017.
[25] Singh H. Two decades with dimorphic chloride intracellular channels (CLICs). FEBS Lett 2010;584:2112–21.
[26] Dahl G, Qiu F, Wang J. The bizarre pharmacology of the ATP release channel pannexin1. Neuropharmacology 2013;0:583–93.
[27] Mijuškovic A, et al. Chloride channels mediate sodium sulphide-induced relaxation in rat uteri. Br J Pharmacol 2015;172:3671–86.
[28] Ye ZC, Oberheim N, Kettenmann H, Ransom BR. Pharmacological "cross-inhibition" of connexin hemichannels and swelling activated anion channels. Glia 2009;57:258–69.
[29] Ponnalagu D, Singh H. Anion channels of mitochondria. Handb Exp Pharmacol 2017;240:71–101.
[30] Skaper SD, Facci L, Giusti P. Intracellular ion channel CLIC1: involvement in microglia-mediated β-amyloid peptide(1-42) neurotoxicity. Neurochem Res 2013;38:1801–8.
[31] Littler DR, et al. Crystal structure of the soluble form of the redox-regulated chloride ion channel protein CLIC4. FEBS J 2005;272:4996–5007.
[32] Pettersen EF, et al. UCSF Chimera - a visualization system for exploratory research and analysis. J Comput Chem 2004;25:1605–12.
[33] Adeniji EA, Olotu FA, Soliman M. Exploring the lapse in druggability: sequence analysis, structural dynamics and binding site characterization of K-RasG12C variant, a feasible oncotherapeutics target. Anticancer Agents Med Chem 2018;18.
[34] Harrop SJ, et al. Crystal structure of a soluble form of the intracellular chloride ion channel CLIC1 (NCC27) at 1.4-A resolution. J Biol Chem 2001;276:44993–5000.
[35] Balmith M, Soliman MES. Potential Ebola drug targets – filling the gap: a critical step forward towards the design and discovery of potential drugs. Biologia 2017;72:1–13.
[36] Chetty S, Soliman MES. Possible allosteric binding site on Gyrase B, a key target for novel anti-TB drugs: Homology modelling and binding site identification using molecular dynamics simulation and binding free energy calculations. Med Chem Res 2015;24:2055–74.
[37] Broomhead NK, Soliman ME. Can we rely on computational predictions to correctly identify ligand binding sites on novel protein drug targets? Assessment of binding site prediction methods and a protocol for validation of predicted binding sites. Cell Biochem Biophys 2017;75:15–23.
[38] Nyamai DW, Bishop ÖT. Aminoacyl tRNA synthetases as malarial drug targets: a comparative bioinformatics study. Malar J 2019;18.
[39] Halgren TA. Identifying and characterizing binding sites and assessing druggability. J Chem Inf Model 2009;49:377–89.
[40] Jiménez J, Doerr S, Martínez-Rosell G, Rose AS, De Fabritiis G. DeepSite: protein-binding site predictor using 3D-convolutional neural networks. Bioinformatics 2017;33:3036–42.
[41] Ngan CH, et al. FTMAP: extended protein mapping with user-selected probe molecules. Nucleic Acids Res 2012;40:W271.
[42] Volkamer A, Kuhn D, Rippmann F, Rarey M. Dogsitescorer: a web server for automatic binding site prediction, analysis and druggability assessment. Bioinformatics 2012;28:2074–5.
[43] Konc J, Janežič D. ProBiS-ligands: a web server for prediction of ligands by examination of protein binding sites. Nucleic Acids Res 2014;42:W215–20.
[44] Case, DA. Amber 18. Univ. California, San Fr.; 2018.
[45] Berendsen HJC, Postma JPM, van Gunsteren WF, DiNola A, Haak JR. Molecular dynamics with coupling to an external bath. J Chem Phys 1984;81:3684–90.
[46] Seifert E. OriginPro 9.1: scientific data analysis and graphing software—software review 1552–1552 J Chem Inf Model 2014;54. 1552–1552.
[47] Biovia DS. Discovery studio 2016 client. San Diego Dassault Systèmes; 2016.
[48] Ghattas MA, Raslan N, Sadeq A, Sorkhy M, Al, Atatreh N. Druggability analysis and classification of protein tyrosine phosphatase active sites. Drug Des Dev Ther 2016;10:3197–209.
[49] Cummings ED, Swoboda HD. Digoxin toxicity. StatPearls Publishing; 2021. p. 6.
[50] Tang T, et al. CLICs-dependent chloride efflux is an essential and proximal upstream event for NLRP3 inflammasome activation. Nat Commun 2017;4(8(1)):202.
[51] Liang CC, Park AY, Guan JL. In vitro scratch assay: a convenient and inexpensive method for analysis of cell migration in vitro. Nat Protoc 2007;2:329–33.
[52] Zhong J, et al. Inhibition of CLIC4 enhances autophagy and triggers mitochondrial and ER stress-induced apoptosis in human glioma U251 cells under starvation. PLoS One 2012;7:e39378.
[53] Malik M, et al. Inducible NOS-induced chloride intracellular channel 4 (CLIC4) nuclear translocation regulates macrophage deactivation. Proc Natl Acad Sci USA 2012;109:6130–5.
[54] Xue H, et al. Knockdown of CLIC4 enhances ATP-induced HN4 cell apoptosis through mitochondrial and endoplasmic reticulum pathways. Cell Biosci 2016;6:1–9.
[55] Ponsioen B, van Zeijil L, Langeslag M, Berryman M, Littler D, Jalink K, et al. Spatiotemporal regulation of chloride intracellular channel protein CLIC4 by RhoA. Mol Biol Cell 2019;15(20(22)):4664–72.
[56] Edwards JC, Kahl CR. Chloride channels of intracellular membranes. FEBS Lett 2010;584:2102–11.
[57] Amamuddy OS, et al. Integrated computational approaches and tools for allosteric drug discovery. Int J Mol Sci 2020;21:847.
[58] Fan J, et al. Harnessing reversed allosteric communication: a novel strategy for allosteric drug discovery. J Med Chem 2021;64:17728–43.
[59] Li J, Kim SG. Blenis, rapamycin: one drug, many effects. J. Cell Metab 2019;4(19(3)):373–9.
[60] Wipperman MF, Monstrose DC, Gotto Jr AM, Hajjar DP. Mammalian target of rapamycin: a metabolic rheostat for regulating adipose tissue function and cardiovascular health. Am J Pathol 2019;189(3):492–501.